ACS APPLIED MATERIALS & INTERFACES

www.acsami.org

Research Article

Observation of Highly Anisotropic Thermal Expansion of Polymer Films

Settasit Chaikasetsin,[○] Jun Young Jung,[○] Hongdeok Kim,[○] Brian S. Y. Kim, Jungju Seo, Joonmyung Choi,* Kiho Bae,* and Woosung Park*

Cite This: *ACS Appl. Mater. Interfaces* 2023, 15, 27166−27172

Read Online

ACCESS | Metrics & More | Article Recommendations | Supporting Information

ABSTRACT: While dimensional change under thermal loading dictates various device failure mechanisms in soft materials, the interplay between microstructures and thermal expansion remains underexplored. Here, we develop a novel method to directly probe the thermal expansion for nanoscale polymer films using an atomic force microscope as well as confining active thermal volume. In a model system, spin-coated poly(methyl methacrylate), we find that the in-plane thermal expansion is enhanced by 20-fold compared to that along the out-of-plane directions in confined dimensions. Our molecular dynamics simulations show that the collective motion of side groups along backbone chains uniquely drives the enhancement of thermal expansion anisotropy of polymers in the nanoscale limit. This work unveils the intimate role of the microstructure of polymer films on its thermal−mechanical interaction, paving a route to judiciously enhance the reliability in a broad range of thin-film devices.

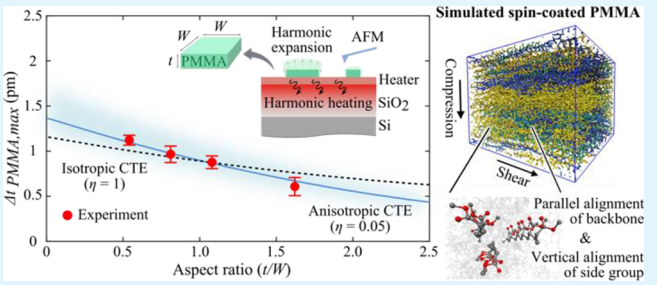

KEYWORDS: *thermal expansion, anisotropy, polymer thin film, microstructure, soft matters*

1. INTRODUCTION

Thermal expansion and the associated thermal stress are the key material properties that dictate the reliability of heterogeneous polymer device applications, such as energy conversion,[1−3] organic thin-film sensors,[4−6] and semiconductor packaging.[7−9] In polymers, a thermal expansion coefficient is intimately connected with their microstructure, including the alignment of backbones and the interactions between neighboring side chains.[10−13] When the thickness of polymers becomes comparable to their gyration length scale, their microstructure is often found to be different from that of the bulk counterpart due to the disentanglement of polymer chains.[14,15] This rearrangement of the microstructures in the thin film limit potentially gives rise to anisotropic properties of polymers, as seen in previous studies for thermal conductivity,[16,17] electrical conductivity,[18,19] and mechanical properties.[20,21] However, experimental challenges as well as the absence of the microscopic model in understanding thermal expansion coefficients of nanoscale polymer films have led to an insufficient understanding of the origin of anisotropy.

One main challenge in probing the anisotropic thermal expansion of polymer films is the uncertain nature of polymer microstructure, which in turn contributes to a significant variation in the experimentally reported values. The key factors that contribute to the uncertainty in the formation of the polymer microstructures can be largely categorized into the extrinsic effects associated with fabrication processes versus the intrinsic effects. On the one hand, the thermal expansion and its anisotropy depend on the inherent polymer structure and properties such as chemical structure,[12,22] chain packing,[23] and molecular weight.[24] For example, the variants of the polyimide (PI) film with the rigid backbone exhibit a higher degree of anisotropy in the coefficient of thermal expansion (CTE) than that of the flexible backbone variants.[12,22] PI variants with denser molecular packing are likely to have smaller CTE due to the restricted motion from densely packed chains.[23] On the other hand, the fabrication process rearranges the microstructure of polymers due to externally applied forces. For instance, between the spin casting and solution shearing process, shear stress is applied differently to the film leading to a variation of backbone chain alignment in polymer microstructure, thereby affecting the properties, as seen in electrical conductivity.[25] Spin coating, a common thin-film processing, often induces anisotropic material behaviors.[13] While many previous studies suggest that spin-coated films show anisotropic CTE depending on the fabrication parameters, these studies are limited to micron-scale-thick films. In nanoscale

Received: March 15, 2023
Accepted: May 18, 2023
Published: May 29, 2023

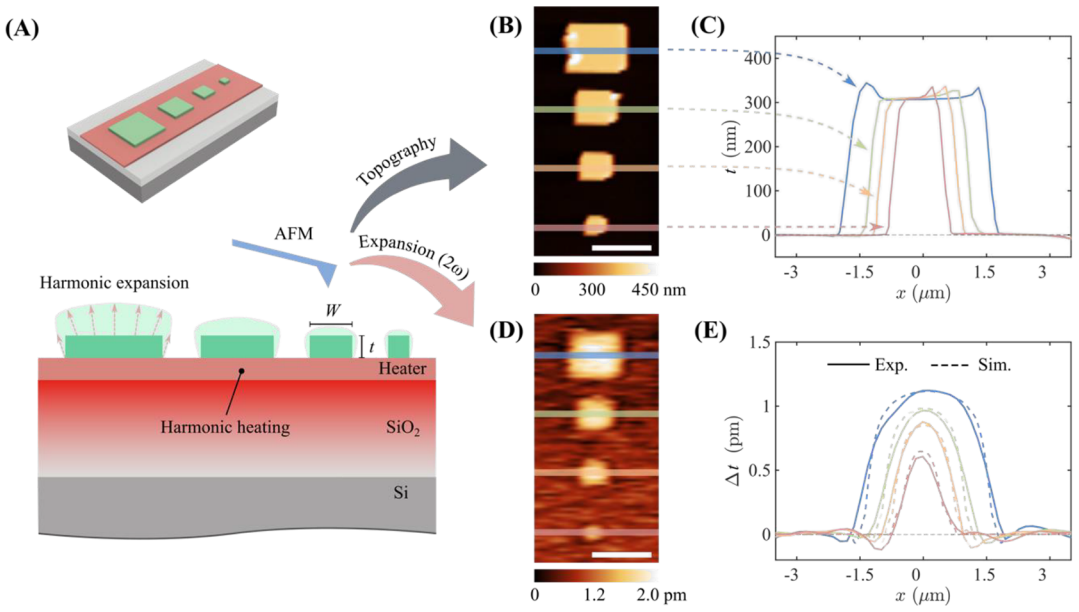

Figure 1. CTE anisotropy measurement via the varying pillar expansion profiles. (A) Schematic for the measurement of the anisotropy in thermal expansion of the PMMA thin film using AFM with the harmonic Joule heating technique. To capture relative in- and out-of-plane expansion, the pillars are patterned to have various aspect ratios (t/W). (B) Topography of four pillars with widths of 3, 2, 1.5, and 1 μm corresponding to aspect-ratios of 0.10, 0.15, 0.20, and 0.30, respectively − a scale bar is 3 μm. (C) Area-averaged line scan of topography over each pillar with an averaged film height of 324.0 ± 0.5 nm − lines plotted in blue, green, orange, and red corresponding to 3, 2, 1.5, and 1 μm pillars in (B), respectively. (D) Thermal expansion graphs of four pillars − scale bar is 3 μm. (E) (solid line) Area-averaged line scan of the harmonic expansion signal over each pillar together with a comparison from (dashed line) profiles from simulation − lines plotted in blue, green, orange, and red corresponding to 3, 2, 1.5, and 1 μm pillars in (D), respectively.

films, the anisotropic nature of CTE can be drastically modified. As the polymer thickness becomes comparable to the gyration length, polymer chains are prone to get disentangled from neighboring chains,[14,26] resulting in the rearrangement of microstructures. However, isotropic thermal expansion characteristics have been typically assumed thus far for polymer thin films even at the nanoscale without sufficient experimental evidence.

Another relevant experimental challenge is the predominant impact of the substrate on the experimental signal. The film expansion measurement is subject to increasing uncertainty with decreasing film thickness as thermal expansion is proportional to its dimension. While methodologies vary, previous work predominantly focuses on micron-scale polymer films due to the limited measurement sensitivity.[11,22,27,28] Our previous work demonstrates a systematical methodology to probe the expansion of nanoscale films with extreme sensitivity by locally confining a thermally active region to the film of interest.[29] In addition, thin films are typically placed on a substrate because of mechanical integrity and stability as it is too thin to stand alone. The adhesion between the film and the substrate often causes additional experimental complexity in the form of film expansion restriction due to the substrate.[30,31] This substrate restriction causes the coupling between in- and out-of-plane CTEs. This effect is particularly pronounced at the nanoscale, and the thermal expansion must be understood in consideration of its substrate.[30,32,33] Existing approaches to minimize the substrate effects include placing films on a liquid substrate for in-plane CTE measurement.[34] But this approach has limited applicability as it requires the removal of substrates. Despite the above-mentioned efforts, a universal method to capture anisotropy in CTE is absent, rendering the physics of thermomechanical interactions underexplored, especially for nanoscale films.

In this paper, we develop a novel method to characterize the anisotropy in thermal expansion coefficients for polymer thin films at the nanoscale. Note that anisotropy of CTE is defined to be

$$\eta = \alpha_{\perp}/\alpha_{\parallel} \tag{1}$$

where η is the CTE anisotropy, $\alpha_{\perp}$ is the out-of-plane CTE, and $\alpha_{\parallel}$ is the in-plane CTE. To account for substrate restriction to decouple in- and out-of-plane CTEs, we modulate the ratio of the lateral expansion to the vertical ones by measuring the thermal expansion of micropatterns without removing the physical substrate support. To capture a marginal thermal expansion of polymer thin films, we confine active thermal volume using harmonic heating, and the associated thermal expansion is captured using atomic force microscopy (AFM). As a sample material, we use poly(methyl methacrylate) (PMMA), which has been considered to be isotropic in thermal expansion coefficients and can be patterned using electron beam lithography. Combining the experimental data with a numerical model, we determine the anisotropy of polymer thin films. Finally, we employ molecular dynamics (MD) simulation to investigate the origin of anisotropy for spin-coated thin films.

The PMMA samples are micropatterned on top of a metal heater, which is placed on a 2.8 μm-thick SiO_2 layer to confine harmonic heating (see sample fabrication details in the Methods section). The aspect ratio of the pillar structure is defined by a film thickness (t) over width (W), t/W, and it ranges from 0.1 to 0.3 as illustrated in Figure 1A. The varying aspect ratios (t/W) enable the decoupling of CTE components

https://doi.org/10.1021/acsami.3c03728
ACS Appl. Mater. Interfaces 2023, 15, 27166−27172

in the in- and out-of-plane directions. The details of the heater fabrication are documented elsewhere.[29]

To obtain the CTEs, we determine the temperature perturbation, film thickness, and corresponding film thermal expansion. The experimental details are well-documented in our earlier work.[29] Briefly, the harmonic Joule heating is applied to a metal heater confining the active thermal volume of interest; meanwhile, the corresponding thermal harmonic expansion and topography signals are obtained through contact-mode AFM as shown in Figure 1A. We represent the CTE tensor in a reduced form consisting of only principal axis components with one axis oriented in the out-of-plane direction and the other two equivalent axes arbitrarily aligned in the in-plane direction.[35] Accordingly, the out-of-plane CTE can be defined as

$$\Delta t(\alpha_\perp, \eta, \nu)/t = \alpha_\perp \Delta T_{2\omega} \quad (2)$$

where Δt, ν, t, ω, and $\Delta T_{2\omega}$ are out-of-plane film expansion, Poisson's ratio, film thickness, harmonic frequency of the heating signal, and harmonic temperature perturbation, respectively. Note that we include the contribution of the in-plane CTE in the out-of-plane film expansion via CTE anisotropy. Harmonic temperature perturbation, $\Delta T_{2\omega}$, is obtained through the 3ω thermometry[36,37] and found to be ~0.074 K (see harmonic temperature perturbation details in the Methods section). This harmonic heating is well confined within the substrate as the thermal diffusion lengths for both SiO_2 and Si calculated from $\sqrt{D/2\omega}$, where D is a thermal diffusivity, are estimated to be ~8 and ~84 μm, respectively.

Using a differential method between the areas with and without PMMA of the topography image as shown in Figure 1B, we separate the substrate effect and simultaneously obtain the film thickness and the out-of-plane film expansion. The area-averaged line scans in each pillar after being subtracted by the substrate signal are plotted in Figure 1C with the average film thickness among all pillars being 324.0 ± 0.5 nm. With the 2ω signal being tracked and captured by AFM and the lock-in amplifier, the harmonic out-of-plane thermal expansion is measured (see harmonic thermal expansion details in the Methods section). Figure 1D shows the 2ω thermal expansion image obtained simultaneously with the topography image in Figure 1B. Note that the signal is converted into a distance unit using a force−distance curve of the AFM cantilever with a conversion factor of ~103.8 mV/nm. The area-averaged line scan of the expansion signals in each pillar after being subtracted by the substrate signal is plotted in Figure 1E in a similar fashion to the topography.

Figure 1E reveals an outstanding trend among the pillars as the maximum out-of-plane film expansion (Δt_{max}) decreases as the pillar aspect ratio increases or equivalently, as pillar width decreases. This confirms the physical behavior of the thin film that the out-of-plane expansion is affected by the in-plane stress contribution; the more in-plane restriction the film has, the higher the out-of-plane expansion becomes. Subsequently, we obtain the best fit for both isotropic and anisotropic CTEs using a numerical model and a regression analysis. Specifically, we simulate numerical finite-element models using a COMSOL with varying values of out-of-plane CTE, CTE anisotropy, aspect ratio, and Poisson's ratio. In each case, the trend line between the maximum film expansion and aspect ratio is found through the regression analysis. We identify the best match CTE and CTE anisotropy from the case with the highest R-squared (R^2) between the simulated and measured data (see the Supplementary Material for the numerical simulation). In addition, we show that this anisotropic CTE gives an agreement of film expansion profiles between simulation and measurement with deviations less than ~8%, as shown in Figure 1E.

2. RESULTS

We emphasize the impact of the CTE anisotropy by comparing the anisotropic and isotropic CTE best-fit cases in the blue solid and dashed lines, respectively, as shown in Figure 2.

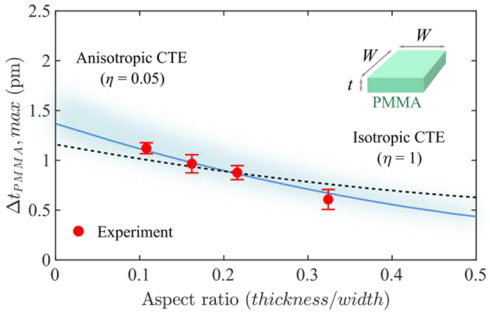

Figure 2. Measured pillar expansions described by anisotropic CTE. Measured maximum out-of-plane film expansion (red circle) for different pillar aspect ratios exhibits a high CTE anisotropy as seen from the best fit case of the anisotropic CTE simulation (blue solid line: $\alpha_\perp$ = 1.48 × 10^{-6} K^{-1}, η = 0.05, ν = 0.45) in contrast to the isotropic CTE case (dotted line: α = 17.3 × 10^{-6} K^{-1}, η = 1, ν = 0.45). The blue overlay band depicts ±10% variation in CTE anisotropy from the best fit case (η = 0.05). (Inset) Pillar dimension schematic.

Assuming isotropic characteristics, the CTE is estimated to be 17.30 × 10^{-6} ± 1.60 × 10^{-6} K^{-1}, which is comparable to that with a similar molecular weight, ranging from ~55 × 10^{-6} to ~100 × 10^{-6} K^{-1} for bulk[38,39] and thin films.[24,29,34,40] The out-of-plane CTE, in-plane CTE, and CTE anisotropy of thin PMMA film are estimated to be 1.48 × 10^{-6} ± 0.13 × 10^{-6} K^{-1}, 29.90 × 10^{-6} ± 2.60 × 10^{-6} K^{-1}, and 0.050 ± 0.002, respectively. The best-fit anisotropic CTE with R^2 of ~0.97 shows a reasonable match with the experimental data within the measurement uncertainty, while the best-fit for isotropic CTE only shows R^2 of ~0.73. Such strong anisotropy is experimentally found for the first time, while PMMA has been considered isotropic in much of previous work. The reported uncertainty propagates from the measured quantities in the measurement such as film thickness, film expansion, temperature rise, and in the calculation including Poisson's ratio (see the Supplementary Material for the uncertainty analysis). In addition, the maximum film expansion dependence on CTE anisotropy is depicted as the overlay band in Figure 2 as the CTE anisotropy is varied by ±10% from the optimal value with the lower and upper bound of 0.045 and 0.055, respectively. Similar anisotropy for spin-coated polymers is found in other material properties including thermal conductivity in PI.[16]

3. DISCUSSION

We attribute the observed anisotropy in the CTE of PMMA films to the microstructural rearrangement of polymer chains induced by the spin-coating process. The spin-coating process contains two key steps: the spinning process of PMMA solution and the evaporation of solvent during baking. The

https://doi.org/10.1021/acsami.3c03728
ACS Appl. Mater. Interfaces 2023, 15, 27166−27172

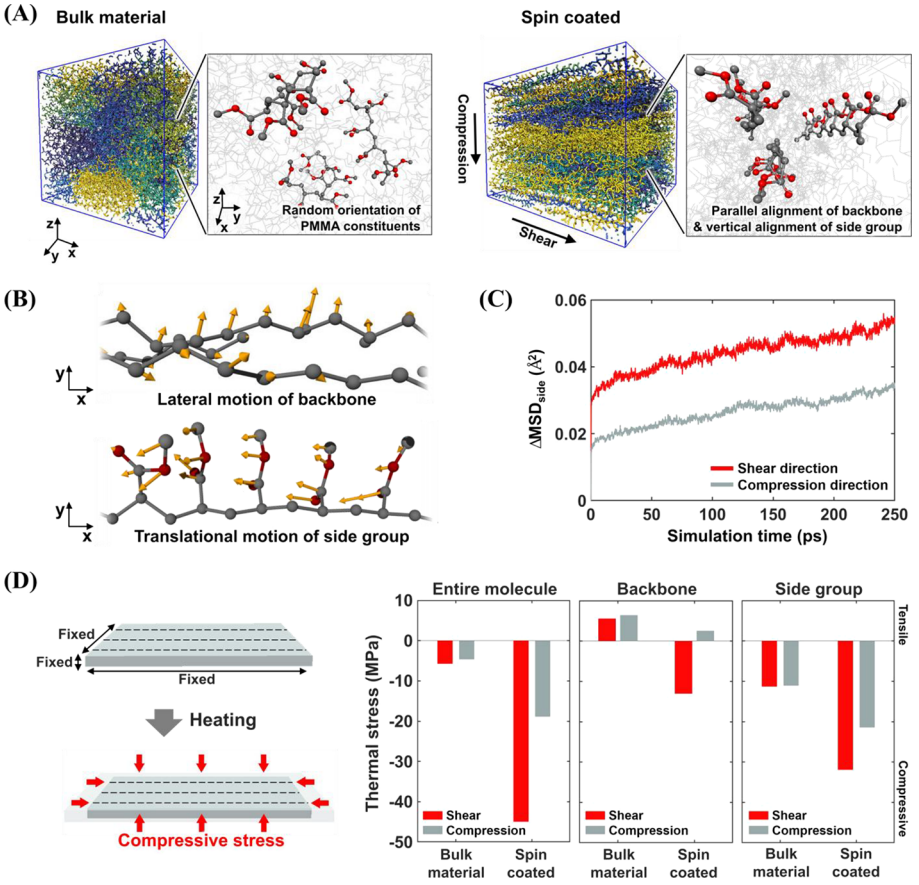

Figure 3. Computational interpretation of anisotropic thermal expansion of the spin-coated PMMA. (A) Description of bulk material and the spin-coated polymer reproduced in a molecular dynamics environment (colored by molecules) and the representative snapshots of their molecular orientations. The hydrogen atoms are hidden for clarity. (B) Key snapshots of atomic oscillation under thermodynamic equilibrium. (C) Effective mean square displacement of the side group (ΔMSD_{side}). (D) Thermal-induced stress analysis of bulk and spin-coated PMMA; total stress combines backbone and side group components.

spinning process exerts a shear stress on the polymer chains near the surface,[41] whereas the evaporation process introduces compressive force via a microscopic capillary action.[41,42] To understand the resultant microstructure of spin-coated film upon these two steps, we perform MD simulation for PMMA by taking into account both the external shear and compressive stresses discussed above. We note that MD simulation only captures microstructural behavior at the molecular level.

We perform all-atom MD simulations for both bulk and spin-coated PMMA films, and their microstructures are illustrated in Figure 3A. A periodic unit cell is constructed with PMMA chains composed of 512 monomers, and the unit cell at thermal equilibrium is used for the bulk PMMA as a reference. For the spin-coated film, both the shear and compressive stress are applied on the bulk unit cell in the *x*- and *z*-directions, respectively (see the Supplementary Material for modeling details and related structural analysis results). In the bulk limit of PMMA, the backbone atoms are randomly oriented. In contrast, the polymer chains in spin-coated films are preferentially aligned along the shear direction with their side groups being orthogonally oriented with respect to the main chains. The more the molecular backbones get aligned, the more the isotactic units get populated in the PMMA chains, which creates a preferred orientation for both the backbone and side group in spin-coated PMMA.

We further investigate the impact of dissimilar microstructures of bulk and spin-coated PMMA films on the nature of thermal expansion. For the spin-coated films, side groups display a collective translational motion along the shear direction at thermal equilibrium as shown in Figure 3B, while the backbones exhibit lateral oscillation with respect to their alignment. Such isotactic side groups particularly facilitate a collective motion along the shear direction (in-plane direction). To quantitatively capture such a preferred motion of polymers, we estimate the mean square displacement (MSD) profiles of the collective oscillation of PMMA molecules (see the Supplementary Material for the details of MSD calculations). Specifically, we calculate ΔMSD_{side}, which represents the net collective motion of side groups without any translational movement of the backbones. Our calculations show a dominant motion in the shear direction, corroborating the increased mobility of side groups along the shear direction (Figure 3C).

The increased mobility of side groups along the shear direction is further quantified by simulating internal stress under thermal loading. Note that the isovolumetric condition is applied to avoid the unnatural annealing effect of the cell. As seen in Figure 3D, the additional kinetic energy of 25 K is applied on both the bulk and the spin-coated PMMA films making the total kinetic energy of 325 K, and we quantify the induced stress under isovolumetric conditions. To maintain the isovolumetric conduction, the thermal oscillation of constituent atoms in response to the applied thermal energy is converted into compressive stress on the unit cell. While the

https://doi.org/10.1021/acsami.3c03728
ACS Appl. Mater. Interfaces 2023, 15, 27166−27172

total thermal stress in the bulk shows an isotropic stress profile, the spin-coated PMMA shows a highly anisotropic profile along the shear direction (in-plane direction). Such an anisotropic stress profile agrees with the preferential ΔMSD_{side} observed along the shear direction in our simulations.

From our simulations, we can deduce that a preferentially larger thermal expansion observed along the shear direction can be attributed to the closely packed isotactic side groups. Namely, their increased shear mobility collectively results in enhanced long-range vibrational interactions, and thereby enhanced thermal expansion along the same shear direction. We emphasize that our simulations suggest the origin of highly anisotropy thermal expansion of the PMMA thin film at the molecular level. We further note that the proportion of side groups far exceeds that of backbone groups in terms of the atomic composition in PMMA chains (26.7% in the backbone to 73.3% in the side group based on molecular weight). The increased role of the side groups is potentially attributed to the side group's larger portion of the total molecular weight.

To gain further insights into the degree of CTE anisotropy of PMMA film in this work, we compare it to the PI film which is known to exhibit anisotropy in CTE. We set up shear stress induced by spinning as a key variable since it affects the arrangement of polymer chains. We estimate the shear stress to be $\tau \sim \mu\omega_{spin}$, where μ (N·s/m^2) is the dynamic viscosity of the polymer solution before spin coating and ω_{spin} (s^{-1}) is the spin coating speed. Figure 4 depicts the plot of CTE anisotropy

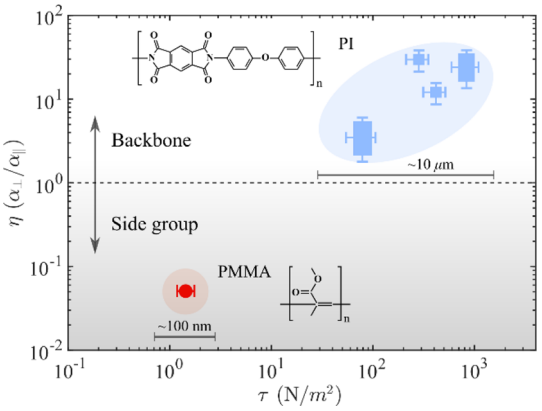

Figure 4. CTE anisotropy as a function of the shear stress from the spin coating process. Red solid circle (PMMA film, this work) and blue solid boxes (PI films[11,12,22,27]); (dashed line) isotropic CTE line (η = 1). Also shown is the qualitative trend of anisotropy in the proportion of backbone and side groups of PI and PMMA. (Top inset) The representative repeating unit of PI (PMDA-ODA). (Bottom inset) PMMA repeating unit.

against the spin-coating shear stress of each PI film[11,12,22,27] and current work PMMA film (see the Supplementary Material for the spin-coating shear stress calculation). In PI films, CTE anisotropy shows a dependency on the spin coating shear stress. The higher the shear stress, the more in-plane-oriented PI backbone chains become, resulting in the higher out-of-plane expansion (η > 1). Dissimilarly, this work PMMA film shows the opposite trend. According to the MD simulation, the PMMA thin film is likely to have a dominant motion under thermal loading from the isotactic side group arrangement, not from the backbone arrangement as seen in PI films, supporting its higher in-plane expansion (η < 1). In addition, we believe that the proportion of backbone and side group of polymers also plays a role in determining the major thermal expansion direction and CTE anisotropy of polymer thin films as demonstrated by PI and PMMA films in Figure 4.

4. CONCLUSIONS

Our work provides a novel method to probe both out-of-plane and in-plane CTEs for polymer films. Specifically, we directly measure a harmonic thermal expansion under a harmonic Joule heating using AFM, and with the varying aspect-ratio pillars, we decouple CTE in- and out-of-plane thermal expansion coefficients in combination with numerical simulations. As a sample material, PMMA is chosen, and the out-of-plane CTE, in-plane CTE, and CTE anisotropy are found to be $1.48 \times 10^{-6} \pm 0.13 \times 10^{-6}$ K^{-1}, $29.90 \times 10^{-6} \pm 2.60 \times 10^{-6}$ K^{-1}, and 0.050 ± 0.002, respectively. While bulk PMMA is typically considered to be isotropic, such significant anisotropy is mainly due to its fabrication process, spin-coating. The effect of spin-coating on PMMA microstructure rearrangement is investigated by molecular dynamics simulations. We introduce shear stress and compression on the computational domain, corresponding to spinning and solvent evaporation steps, respectively. We find that such rearrangement of microstructure potentially induces a significant anisotropy in thermal expansion coefficients. Specifically, the isotactic arrangement of PMMA side groups in the spin-coated film exhibits relatively high in-plane motion which dominates the thermal expansion behavior. The nanoscale PMMA film demonstrates significant anisotropic thermal expansion while its bulk counterpart is considered to be isotropic. Such a significant mismatch is attributed to microstructure arrangement, which is pronounced in nanoscale films where chains are less entangled.

5. METHODS

5.1. Sample Fabrication. The Si wafer substrate is cleaned using standard organic, particle, and ionic clean processes, followed by a thermal oxidation process to grow approximately 2.8 μm-thick SiO_2. The 15 μm-wide and 40 nm-thick Pt metal heater lines are patterned using a maskless lithography system (Heidelberg Instruments), electron beam evaporation, and metal lift-off processes. Subsequently, a 20 nm-thick Al_2O_3 is deposited uniformly onto the substrate by atomic layer deposition to screen the electric field from the heater, followed by 20 μm-wide and 60 nm-thick Pt ground lines patterned similarly to the heater layer to provide electrical ground. PMMA 950 K A4 (with a molecular weight of 950 kg/mol and 4% Anisole) resist variant from Microchem is used in this experiment as it is considered a common and high-throughput resist in many electron-beam lithography applications. The sample is spin-coated with PMMA at 2000 rpm and then prebaked at 200 °C for 2 min to evaporate the solvent. The PMMA film is e-beam-patterned into pillar shapes by exposing the surrounding area around the desired pattern and developed using methyl isobutyl ketone.

5.2. Harmonic Temperature Perturbation. The harmonic temperature rise in the second harmonic is obtained from $\Delta T_{2\omega} = V_{3\omega}/(I_{RMS}R_o\alpha_{TCR})$, where $V_{3\omega}$, I_{RMS}, R_o, and α_{TCR} are the 3ω voltage signal, root-mean-square current, resistance at room temperature of the heater, and temperature coefficient of resistance (TCR) of the heater, respectively. The Pt heater is estimated to have R_o of ~431 Ω and α_{TCR} of ~0.002 K^{-1} and the harmonic signal of 2 mA root-mean-square current at 1 kHz gives a harmonic temperature perturbation, $\Delta T_{2\omega}$, of ~0.074 K.

5.3. Harmonic Thermal Expansion. The out-of-plane film expansion in the form of harmonic thermal expansion is measured by synchronizing the oscillation of the AFM signal with the harmonic heating frequency through the lock-in amplifier. Harmonic Joule heating generates power in the second harmonic frequency (2ω) corresponding to $P_{AC} = V_0^2(1 - \cos(2\omega t))/2R$, where P_{AC}, V_0, and R

https://doi.org/10.1021/acsami.3c03728
ACS Appl. Mater. Interfaces 2023, 15, 27166−27172

are the generated power, the magnitude of the applied voltage, and heater electrical resistance, respectively.

■ ASSOCIATED CONTENT

Data Availability Statement

The data that support the findings of this study are available from the corresponding author upon reasonable request.

Supporting Information

The Supporting Information is available free of charge at https://pubs.acs.org/doi/10.1021/acsami.3c03728.

Additional experimental details, simulation details, and methods, including uncertainty and spin-coating shear stress calculations (PDF)

■ AUTHOR INFORMATION

Corresponding Authors

Joonmyung Choi − *Department of Mechanical Design Engineering, Hanyang University, Seoul 04763, Korea; Department of Mechanical Engineering, BK21 FOUR ERICA-ACE Center, Hanyang University, Ansan 15588, Korea;* orcid.org/0000-0003-3673-8069; Email: joonchoi@hanyang.ac.kr

Kiho Bae − *Department of Energy Engineering, Korea Institute of Energy Technology, Naju 58217, Korea*; Email: kbae@kentech.ac.kr

Woosung Park − *Department of Mechanical Engineering, Sogang University, Seoul 04107, Korea*; Email: wspark@sogang.ac.kr

Authors

Settasit Chaikasetsin − *Department of Mechanical Engineering, Stanford University, Stanford, California 94305, United States;* orcid.org/0000-0003-4661-0878

Jun Young Jung − *Science Instrumentation Assessment and Application Team, Korea Basic Science Institute, Daejeon 34133, South Korea*

Hongdeok Kim − *Department of Mechanical Design Engineering, Hanyang University, Seoul 04763, Korea; Department of Mechanical Engineering, BK21 FOUR ERICA-ACE Center, Hanyang University, Ansan 15588, Korea*

Brian S. Y. Kim − *Department of Mechanical Engineering, Columbia University, New York, New York 10027, United States*

Jungju Seo − *Science Instrumentation Assessment and Application Team, Korea Basic Science Institute, Daejeon 34133, South Korea*

Complete contact information is available at: https://pubs.acs.org/10.1021/acsami.3c03728

Author Contributions

○S.C., J.Y.J., and H.K. equally contributed to this work.

Notes

The authors declare no competing financial interest.

■ ACKNOWLEDGMENTS

The authors thank Professor Fritz Prinz (Stanford University) and Professor Turgut Gür (Stanford University) for their helpful suggestions on the manuscript. This work is supported by a National Research Foundation of Korea (NRF) grant funded by the Korea government (Ministry of Science and ICT) (No. 2021R1C1C1008693). This work was supported by the National Research Foundation of Korea (NRF) grant funded by the Korea government (MSIT) (No. RS-2023-00210865). Part of this work is performed at the Stanford Nano Shared Facilities (SNSF), supported by the National Science Foundation under award ECCS-2026822.

■ REFERENCES

(1) Banerjee, T.; Podjaski, F.; Kröger, J.; Biswal, B. P.; Lotsch, B. V. Polymer Photocatalysts for Solar-to-Chemical Energy Conversion. *Nat. Rev. Mater.* **2021**, *6*, 168−190.

(2) Hyeon, D. Y.; Nam, C.; Ham, S. S.; Hwang, G. T.; Yi, S.; Kim, K. T.; Park, K. I. Enhanced Energy Conversion Performance of a Magneto−Mechano−Electric Generator Using a Laminate Composite Made of Piezoelectric Polymer and Metallic Glass. *Adv. Electron. Mater.* **2021**, *7*, No. 2000969.

(3) Gu, C.; Huang, N.; Chen, Y.; Qin, L.; Xu, H.; Zhang, S.; Li, F.; Ma, Y.; Jiang, D. π-Conjugated Microporous Polymer Films: Designed Synthesis, Conducting Properties, and Photoenergy Conversions. *Angew. Chem., Int. Ed.* **2015**, *54*, 13594−13598.

(4) Nketia-Yawson, B.; Noh, Y. Y. Organic Thin Film Transistor with Conjugated Polymers for Highly Sensitive Gas Sensors. *Macromol. Res.* **2017**, *25*, 489−495.

(5) Zhao, C.; Li, L.-Y.; Guo, M.-M.; Zheng, J. Functional Polymer Thin Films Designed for Antifouling Materials and Biosensors. *Chem. Pap.* **2012**, *66*, 323−339.

(6) Bang, J.; Lee, W. S.; Park, B.; Joh, H.; Woo, H. K.; Jeon, S.; Ahn, J.; Jeong, C.; Kim, T.i.; Oh, S. J. Highly Sensitive Temperature Sensor: Ligand-Treated Ag Nanocrystal Thin Films on PDMS with Thermal Expansion Strategy. *Adv. Funct. Mater.* **2019**, *29*, No. 1903047.

(7) Zhu, L.; Li, Y.; Han, S.; Niu, H.; Wu, D.; Qi, S. Revealing the High-Modulus Mechanism of Polyimide Films Prepared with 3,4′-ODA. *Polymers* **2021**, *13*, 3175.

(8) Phua, E. J. R.; Liu, M.; Cho, B.; Liu, Q.; Amini, S.; Hu, X.; Gan, C. L. Novel High Temperature Polymeric Encapsulation Material for Extreme Environment Electronics Packaging. *Mater. Des.* **2018**, *141*, 202−209.

(9) Li, R.; Yang, X.; Li, J.; Shen, Y.; Zhang, L.; Lu, R.; Wang, C.; Zheng, X.; Chen, H.; Zhang, T. Review on Polymer Composites with High Thermal Conductivity and Low Dielectric Properties for Electronic Packaging. *Mater. Today Phys.* **2022**, *22*, No. 100594.

(10) Numata, S.; Oohara, S.; Fujisaki, K.; Imaizumi, J.; Kinjo, N. Thermal Expansion Behavior of Various Aromatic Polyimides. *J. Appl. Polym. Sci.* **1986**, *31*, 101−110.

(11) Elsner, G.; Kempf, J.; Bartha, J. W.; Wagner, H. H. Anisotropy of Thermal Expansion of Thin Polyimide Films. *Thin Solid Films* **1990**, *185*, 189−197.

(12) Pottiger, M. T.; Coburn, J. C.; Edman, J. R. The Effect of Orientation on Thermal Expansion Behavior in Polyimide Films. *J. Polym. Sci., Part B: Polym. Phys.* **1994**, *32*, 825−837.

(13) Chan, J. M.; Wang, M. Visualizing the Orientation of Single Polymers Induced by Spin-Coating. *Nano Lett.* **2022**, *22*, 5891−5897.

(14) Aoki, H.; Morita, S.; Sekine, R.; Ito, S. Conformation of Single Poly(Methyl Methacrylate) Chains in an Ultra-Thin Film Studied by Scanning near-Field Optical Microscopy. *Polym. J.* **2008**, *40*, 274−280.

(15) Arita, H.; Mitamura, K.; Kobayashi, M.; Yamada, N. L.; Jinnai, H.; Takahara, A. Chain-Mixing Behavior at Interface between Polystyrene Brushes and Polystyrene Matrices. *Polym. J.* **2013**, *45*, 117−123.

(16) Kurabayashi, K.; Asheghi, M.; Touzelbaev, M.; Goodson, K. E. Measurement of the Thermal Conductivity Anisotropy in Polyimide Films. *J. Microelectromechanical Syst.* **1999**, *8*, 180−191.

(17) Pan, X.; Debije, M. G.; Schenning, A. P. H. J. High Thermal Conductivity in Anisotropic Aligned Polymeric Materials. *ACS Appl. Polym. Mater.* **2021**, *3*, 578−587.

(18) Ohnuma, H.; Hasegawa, K.; Se, K.; Kotaka, T. Anisotropic Electrical Conductivity of Oriented Poly(Diacetylene) Films. *Macromolecules* **1985**, *18*, 2339−2341.
(19) Nardes, A. M.; Kemerink, M.; Janssen, R. A. J.; Bastiaansen, J. A. M.; Kiggen, N. M. M.; Langeveld, B. M. W.; van Breemen, A. J. J. M.; de Kok, M. M. Microscopic Understanding of the Anisotropic Conductivity of PEDOT:PSS Thin Films. *Adv. Mater.* **2007**, *19*, 1196−1200.
(20) Robin, C. J.; Vishnoi, A.; Jonnalagadda, K. N. Mechanical Behavior and Anisotropy of Spin-Coated SU-8 Thin Films for MEMS. *J. Microelectromechanical Syst.* **2014**, *23*, 168−180.
(21) Ye, C.; Singh, G.; Wadley, M. L.; Karim, A.; Cavicchi, K. A.; Vogt, B. D. Anisotropic Mechanical Properties of Aligned Polystyrene-Block- Polydimethylsiloxane Thin Films. *Macromolecules* **2013**, *46*, 8608−8615.
(22) Liou, H.-C.; Ho, P. S.; Stierman, R. Thickness Dependence of the Anisotropy in Thermal Expansion of PMDA-ODA and BPDA-PDA Thin Films. *Thin Solid Films* **1999**, *339*, 68−73.
(23) Okada, T.; Ishige, R.; Ando, S. Effects of Chain Packing and Structural Isomerism on the Anisotropic Linear and Volumetric Thermal Expansion Behaviors of Polyimide Films. *Polymer* **2018**, *146*, 386−395.
(24) González-Benito, J.; Castillo, E.; Cruz-Caldito, J. F. Determination of the Linear Coefficient of Thermal Expansion in Polymer Films at the Nanoscale: Influence of the Composition of EVA Copolymers and the Molecular Weight of PMMA. *Phys. Chem. Chem. Phys.* **2015**, *17*, 18495.
(25) Worfolk, B. J.; Andrews, S. C.; Park, S.; Reinspach, J.; Liu, N.; Toney, M. F.; Mannsfeld, S. C. B.; Bao, Z. Ultrahigh Electrical Conductivity in Solution-Sheared Polymeric Transparent Films. *Proc. Natl. Acad. Sci. U. S. A.* **2015**, *112*, 14138−14143.
(26) Singh, L.; Ludovice, P. J.; Henderson, C. L. Influence of Molecular Weight and Film Thickness on the Glass Transition Temperature and Coefficient of Thermal Expansion of Supported Ultrathin Polymer Films. *Thin Solid Films* **2004**, *449*, 231−241.
(27) Ree, M.; Chen, K.-J.; Kirby, D. P.; Katzenellenbogen, N.; Grischkowsky, D. Anisotropic Properties of High-temperature Polyimide Thin Films: Dielectric and Thermal-expansion Behaviors. *J. Appl. Phys.* **1992**, *72*, 2014−2021.
(28) Chen, S. T.; Wagner, H. H. Out-of-Plane Thermal Expansion Coefficient of Biphenyldianhydride-Phenylenediamine Polyimide Film. *J. Electron. Mater.* **1993**, *22*, 797−799.
(29) Chaikasetsin, S.; Kodama, T.; Bae, K.; Jung, J. Y.; Shin, J.; Lee, B. C.; Kim, B. S. Y.; Seo, J.; Sim, U.; Prinz, F. B.; Goodson, K. E.; Park, W. Thermal Expansion Characterization of Thin Films Using Harmonic Joule Heating Combined with Atomic Force Microscopy. *Appl. Phys. Lett.* **2021**, *118*, 194101.
(30) Zhong, Y.; Zhang, L.; Park, J.-H.; Cruz, S.; Li, L.; Guo, L.; Kong, J.; Wang, E. N. A Unified Approach and Descriptor for the Thermal Expansion of Two-Dimensional Transition Metal Dichalcogenide Monolayers. *Sci. Adv.* **2022**, *8*, No. eabo3783.
(31) Zoo, Y.; Adams, D.; Mayer, J. W.; Alford, T. L. Investigation of Coefficient of Thermal Expansion of Silver Thin Film on Different Substrates Using X-Ray Diffraction. *Thin Solid Films* **2006**, *513*, 170−174.
(32) Kim, I.; Burzo, M. G.; Komarov, P. L.; Raad, P. E. Thermal Conductivity Measurements of Ultra-Thin Amorphous Poly(Methyl Methacrylate) (PMMA) Films. In *Volume 8C: Heat Transfer and Thermal Engineering*; ASME International Mechanical Engineering Congress and Exposition; American Society of Mechanical Engineers, 2013; p 66507.
(33) Shin, Y.; Lee, H.; Lee, W.; Ryu, D. Y. Glass Transition and Thermal Expansion Behavior of Polystyrene Films Supported on Polystyrene-Grafted Substrates. *Macromolecules* **2016**, *49*, 5291−5296.
(34) Kim, J. H.; Jang, K. L.; Ahn, K.; Yoon, T.; Lee, T. I.; Kim, T. S. Thermal Expansion Behavior of Thin Films Expanding Freely on Water Surface. *Sci. Rep.* **2019**, *9*, 7071.
(35) Belousov, R. I.; Filatov, S. K. Algorithm for Calculating the Thermal Expansion Tensor and Constructing the Thermal Expansion Diagram for Crystals. *Glass Phys. Chem.* **2007**, *33*, 271−275.
(36) Cahill, D. G. Thermal Conductivity Measurement from 30 to 750 K: The 3ω Method. *Rev. Sci. Instrum.* **1990**, *61*, 802−808.
(37) Dames, C. Measuring the Thermal Conductivity of Thin Films: 3 Omega and Related Electrothermal Methods. *Annu. Rev. Heat Transf.* **2013**, *16*, 7−49.
(38) Wilson, J. D.; Treloar, L. R. G. The Anisotropic Thermal Expansivity of Oriented Perspex. *J. Phys. D: Appl. Phys.* **1972**, *5*, 1614−1620.
(39) Wang, L.-H.; Choy, C. L.; Porter, R. S. Thermal Expansion of Oriented Poly(Methyl Methacrylate). *J. Polym. Sci. Polym. Phys. Ed.* **1983**, *21*, 657−665.
(40) Kahle, O.; Wielsch, U.; Metzner, H.; Bauer, J.; Uhlig, C.; Zawatzki, C. Glass Transition Temperature and Thermal Expansion Behaviour of Polymer Films Investigated by Variable Temperature Spectroscopic Ellipsometry. *Thin Solid Films* **1998**, *313-314*, 803−807.
(41) Sahu, N.; Parija, B.; Panigrahi, S. Fundamental Understanding and Modeling of Spin Coating Process: A Review. *Indian J. Phys.* **2009**, *83*, 493−502.
(42) Zhou, J.; Man, X.; Jiang, Y.; Doi, M. Structure Formation in Soft-Matter Solutions Induced by Solvent Evaporation. *Adv. Mater.* **2017**, *29*, No. 1703769.

https://doi.org/10.1021/acsami.3c03728
ACS Appl. Mater. Interfaces 2023, 15, 27166−27172